Journal of Photonics for Energy

SPIEDigitalLibrary.org/jpe

Low-bandgap small molecules for near-infrared photovoltaic applications

M. Ballarotto
W.N. Herman
D.B. Romero

SPIE

Low-bandgap small molecules for near-infrared photovoltaic applications

M. Ballarotto,[a,b] W.N. Herman,[a] and D.B. Romero[a,b]
[a] University of Maryland, Laboratory for Physical Sciences, College Park, Maryland 20740
[b] University of Maryland, Department of Electrical and Computer Engineering, College Park, Maryland 20742
mihaela@lps.umd.edu

Abstract. We investigate the effects of interfacial layers on the photovoltaic properties of bilayer organic heterojunction photovoltaic devices. The devices were fabricated using aluminum phthalocyanine chloride (AlPcCl) as electron donor and fullerene (C_{60}) as electron acceptor. Two types of interfacial layers inserted between the transparent indium-tin-oxide anode and the AlPcCl layer were investigated: PEDOT:PSS and MoO_3. We find that these interfacial layers have a strong influence on the device open-circuit voltage (V_{OC}). The effects of temperature and illumination intensity on V_{OC} were explored. © *2011 Society of Photo-Optical Instrumentation Engineers*. [DOI: 10.1117/1.3528044]

Keywords: organic photovoltaics; surface recombination; interfacial layers; open-circuit voltage.

Paper 10135SSPR received Aug. 15, 2010; revised manuscript received Oct. 14, 2010; accepted for publication Nov. 18, 2010; published online Jan. 4, 2011.

1 Introduction

Aluminum phthalocyanine chloride (AlPcCl) is a low-bandgap ($E_g = 1.56$ eV) small-molecule organic semiconductor that is currently being explored to extend the spectral range of organic photovoltaic devices to the near-infrared. Recent works[1–3] on bilayer organic photovoltaic devices using AlPcCl as the donor molecule combined with C_{60} as the acceptor molecule have demonstrated 2% power conversion efficiency in these devices. In these works, the type of interfacial layer formed at the indium-tin-oxide (ITO) anode was shown to have a strong influence on the device open-circuit voltage (V_{OC}). UV ozone treated ITO substrates manifested substantially different V_{OC} of 0.68 V (Ref. 1) and 0.84 V (Ref. 2). In devices where molydenum oxide (MoO_3) was used as an interfacial layer, $V_{OC} = 0.83$ V has been reported.[3]

In general, the power conversion efficiency (η_P) of a photovoltaic device is given by $\eta_P = V_{OC}J_{SC}FF/P_{in}$ where J_{SC} and FF are the device short-circuit current density and fill factor, respectively, and P_{in} is the incident light intensity. Aside from its direct effect on η_P, V_{OC} is also known to have an influence on FF. Shockley and Queisser[4] were the first to note that FF for an ideal solar cell depends only on the temperature normalized open-circuit voltage, $v_{OC} = V_{OC}/(k_BT/q)$, where T is the cell temperature, k_B is Boltzmann's constant, and q is the electronic charge. Empirical expressions proposed by Green[5] demonstrated that FF increases as v_{OC} is raised. Therefore, in order to optimize the efficiency of AlPcCl-based bilayer organic photovoltaic devices, it is important to understand the observed effects[1–3] of the anode interface on V_{OC}. In the present work, we address the question of whether the device open-circuit voltage is determined by the intrinsic properties of the AlPcCl/C_{60} donor/acceptor heterojunction or the properties of the electrode interfaces. From detailed temperature and power dependence of

1947-7988/2011/$25.00 © 2011 SPIE

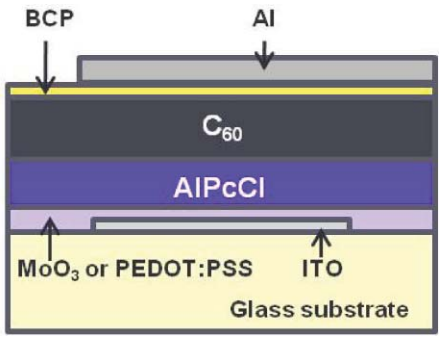

Fig. 1 Structure of the bilayer devices based on small molecules AlPcCl (donor) and C_{60} (acceptor).

the device current density versus voltage characteristics, we show that both factors contribute to the device open-circuit voltage.

2 Device Fabrication and Characterization

The materials used to fabricate our bilayer devices were acquired from various commercial sources. The device geometry is presented in Fig. 1. The substrate is glass covered with transparent conducting ITO (~150 nm thick with sheet resistance $R_s = 4$–$8\ \Omega$ from Delta Technologies). We investigated poly(3,4-ethylenedioxythophene) doped with poly(styrenesulfonate) (PEDOT:PSS) in aqueous solution (Baytron P, H.C. Stark, USA) and MoO_3 (Aldrich, USA) as interfacial hole-transport layers in our devices. Sublimed grade bathocuproine (BCP, Aldrich) was used to form an ohmic contact between C_{60} and the aluminum electrode. AlPcCl (Aldrich) and C_{60} (99.5% purity, nano-C) were used to form the electroactive bilayers of our devices. AlPcCl was purified by thermal gradient sublimation before being used for device fabrication.

The ITO electrodes were first patterned on the glass substrates by photolithographic techniques. The ITO substrates were then cleaned by ultrasonic treatment sequentially in detergent, deionized water, and acetone followed by rinsing in isopropyl alcohol. To ensure a valid comparison of the photovoltaic characteristics of devices with different interfacial layers, substrates covered by PEDOT:PSS and MoO_3 were initially prepared separately. A 50-nm-thick PEDOT:PSS film was spin-coated from the aqueous Baytron P solution onto the ITO/glass at 5000 rpm under ambient atmosphere. The air-dried film was transferred inside a glove box and heated at 150°C for 10 min to remove any residual moisture from the film. A 60-Å MoO_3 thin film was thermally evaporated on another patterned ITO substrate. Both substrates were then loaded into the thermal evaporation system for subsequent depositions of the remaining identical layers in each device comprising the device structure. Films of 220 Å of AlPcCl and 425 Å of C_{60} were thermally evaporated onto the substrates with a base pressure of 2×10^{-6} Torr. The devices were completed by depositing 100 Å of BCP and a 1000 Å Al through a shadow mask defining the 0.05×0.05-in. square active area for the device. The entire device fabrication was carried out inside a nitrogen-filled glove box to avoid potential sources for photo-oxidative degradation.

On completion, the devices were mounted in a cryostat inside the glove box. The mounted device was subsequently taken outside the glove box and pumped to 5×10^{-6} Torr prior to measurement of the current density versus voltage (J–V) characteristics. The measurements were performed over a temperature range of 30–300 K and illumination intensities between 12 and 194 mW/cm^2. The illumination source was a simulated AM 1.5 global solar simulator (Oriel 300 W) with a maximum integrated intensity of ~200 mW/cm^2. The incident illumination intensity was adjusted using different size apertures and by varying the power of the solar simulator. The intensity was measured using an NREL-calibrated silicon photovoltaic cell as detector.

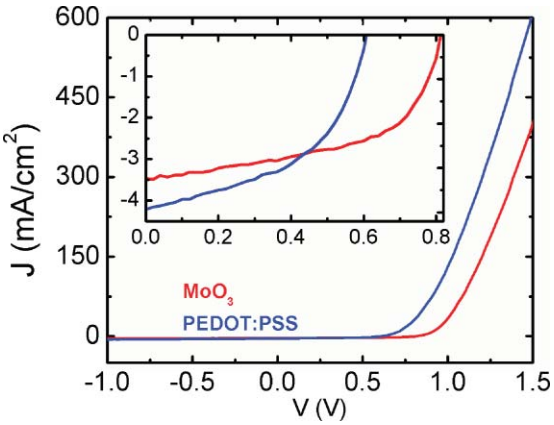

Fig. 2 Room-temperature J_L–V characteristics of AlPcCl/C_{60} heterojunctions with the two types of interfacial layers, MoO_3 and PEDOT:PSS, under AM1.5 global solar simulator with 100 mW/cm^2.

3 Results and Discussions

3.1 *Room-Temperature Current Density versus Voltage Characteristics in the Dark and under Illumination*

Figure 2 presents a comparison of the illuminated current density (J_L) versus voltage (V) characteristics at room temperature of the AlPcCl/C_{60}-based heterojunction photovoltaic devices fabricated with the two types of interfacial layers. We observe a significant increase in the open-circuit voltage from $V_{OC} = 0.61$ V using the PEDOT:PSS interfacial layer to $V_{OC} = 0.81$ V for the device with the MoO_3 layer. The corresponding device fill factor also increased from 0.49 to 0.55. However, the short-circuit current is reduced for the device fabricated with MoO_3 compared to PEDOT:PSS from 4.21 to 3.47 mA/cm^2. Nevertheless, the observed increase in V_{OC} and FF results in a significant improvement in the power-conversion efficiency from 1.33 to 1.64%.

To understand the differences in the J–V characteristics presented in Fig. 2, we use the typical equivalent circuit model developed to describe photovoltaic devices.[6] In this model, the photocell is described by a diode in parallel with a current source, J_{ph}, and a parallel resistance R_p, all connected in series with the resistance R_s. The diode represents the rectifying donor-acceptor heterojunction and is characterized by the reverse-bias saturation current density J_S, and the diode ideality factor n. $J_{ph}(V)$ is the voltage-dependent photogenerated current density present in the device under illumination, and it becomes zero for devices measured in the dark. The parallel resistance R_p is related to leakage currents due to pinholes or other imperfections during device fabrication or to intrinsic recombination processes present in the active layers. The series resistance R_s accounts for the organic layer resistance together with the contact resistance formed between each of the interfaces present in the device. With this model, the current density (J) as a function of the applied voltage is given by the generalized Shockley diode Eq. (1),

$$J = \frac{R_p}{R_s + R_p}\left\{J_s\left[\exp\frac{q(V - JR_s)}{nk_BT} - 1\right] + \frac{V}{R_p}\right\} - J_{ph}(V). \quad (1)$$

Note that Eq. (1) describes the illuminated current density (J_L) when $J_{ph} \neq 0$ and the dark current density (J_d) for $J_{ph} = 0$. In our analysis, we estimate the photocurrent as $J_{ph} = J_L - J_d$.

The experimental J_d versus V curve is fitted to Eq. (1) to obtain the diode parameters R_s, R_p, n, and J_s. The fit to the room temperature $J_d - V$ for both devices is presented in Fig. 3. Good agreement of the fit with the data is obtained using the diode parameters listed in the caption to Fig. 3. When the PEDOT:PSS interfacial layer is replaced with the MoO_3 interfacial layer,

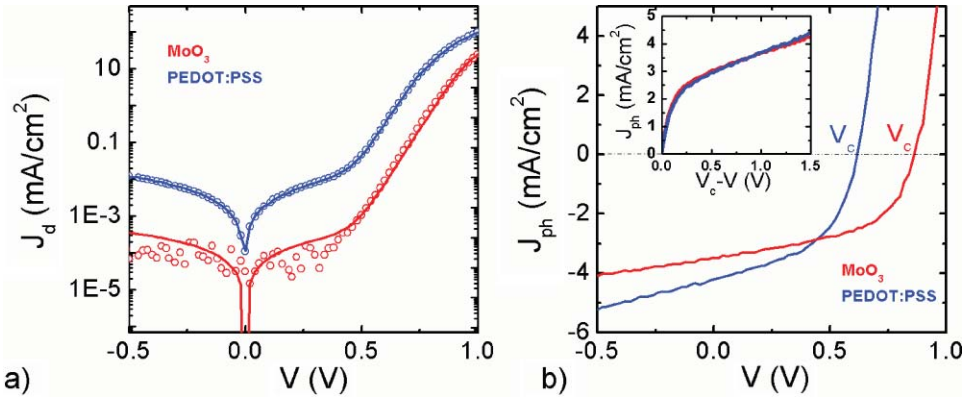

Fig. 3 (a) Dark J_d–V characteristics of AlPcCl/C_{60} heterojunction devices fabricated with two types of interfacial layers: MoO_3 and PEDOT:PSS. The lines represent fits to the data using Eq. (1) with fitting parameters: $J_s = 7.84\times10^{-9}$ mA/cm^2, $n = 1.69$, $R_s = 1.84$ Ω cm^2, $R_p = 1.39$ MΩ cm^2 for the MoO_3 device, and $J_s = 9.48\times10^{-7}$ mA/cm^2, $n = 1.82$, $R_s = 1.36$ Ω cm^2, $R_p = 0.48$ MΩ cm^2 for the PEDOT:PSS device. b) J_{ph}–V characteristics of AlPcCl/C_{60} heterojunction devices fabricated with two types of interfacial layers: MoO_3 and PEDOT:PSS. Inset: J_{ph} as a function of effective applied voltage, V_C–V, where V_C is the compensation voltage defined in the text.

the reverse-bias saturation current J_s decreases by two orders of magnitude from 9.48×10^{-7} mA/cm^2 to 7.84×10^{-9} mA/cm^2. As we will show later, such a decrease in J_s can explain the elevated V_{OC} measured from the device with the MoO_3 interfacial layer.

An expression for the V_{OC} can be extracted from Eq. (1) by setting $J = 0$. For $R_s \ll R_p$ this yields,

$$V_{oc} = \frac{nk_BT}{q}\ln\left(\frac{J_{ph}(V_{oc})}{J_s} + 1 - \frac{V_{oc}}{J_s R_p}\right). \tag{2}$$

The device fill factor can also be calculated from the diode parameters of Eq. (1). In general, FF is obtained numerically. However, the following empirical estimates were previously shown to be good approximations of the numerical values when $V_{OC} > 10nk_BT$[5,6],

$$\begin{aligned} \mathrm{FF_O} &= \frac{v_{OC} - \ln(v_{OC} + 0.72)}{v_{OC} + 1}, \quad (r_S = 1/r_P = 0) \\ \mathrm{FF_S} &= \mathrm{FF_O}\,(1 - 1.1r_S) + 0.19r_S^2, \quad (0 \le r_S \le 0.4,\ 1/r_P = 0) \\ \mathrm{FF} &= \mathrm{FF_S}\left\{1 - \frac{(v_{OC} + 0.7)}{v_{OC}}\frac{\mathrm{FF_S}}{r_P}\right\}, \quad (0 \le r_S + 1/r_P \le 0.4) \end{aligned} \tag{3}$$

where the normalized quantities are defined as $v_{OC} = qV_{OC}/nk_BT$, $r_S = R_s/R_{CH}$, and $r_p = R_p/R_{CH}$. The characteristic resistance is given by $R_{CH} = V_{OC}/J_{SC}$.

We compare the experimentally measured V_{OC} with that given by Eq. (2) using the fitting parameters obtained from the dark current characteristics described above. From Fig. 3(b), we estimate $J_{ph}(V_{OC}) = 1.16$ mA/cm^2 for the MoO_3 device and $J_{ph}(V_{OC}) = 0.31$ mA/cm^2 for the PEDOT:PSS device. Using Eq. (2), and noting that the first term dominates over the other two terms for the quantities inside the bracket, the expected open-circuit voltage for the device with a PEDOT:PSS interface is $V_{OC} = 0.60$ V, whereas the one with a MoO_3 interface has $V_{OC} = 0.82$ V. These estimates are in very good agreement with the experimental values of 0.61 and 0.81 V, respectively, suggesting that the equivalent circuit model is applicable in describing the devices' photovoltaic characteristics at room temperature.

We now account for the observed fill factor in both devices. Using the estimate of V_{OC} derived from the dark diode characteristics, the ideal fill factor (FF_O) calculated from Eq. (3) is $FF_O = 0.80$ for the MoO_3 device and $FF_O = 0.74$ for the PEDOT:PSS device. Correction associated with the different series resistance yields $FF_S = 0.79$ for the MoO_3 device and $FF_S = 0.73$ for the PEDOT:PSS device, demonstrating negligible effect of R_s on FF. The large value of R_p extracted from the dark J_d–V characteristic from both devices also results in negligible correction to the fill factor. However, the linear increase of J_{ph} at large negative applied voltage [seen in Fig. 3(b)] suggests another R_p contribution to FF under illumination condition. Estimating this light-induced parallel resistance from the slope of the linear part of the J_L–V curve, we obtain $R_p \approx 850\ \Omega\ cm^2$ for the MoO_3 device and $R_p \approx 538\ \Omega\ cm^2$ for the PEDOT:PSS device. Using these values, the fill factor calculated from Eq. (3) is $FF = 0.61$ for the MoO_3 device and $FF = 0.55$ for the PEDOT:PSS device, values that are comparable to the corresponding measured device fill factor. This analysis shows that FF is controlled by the ideality factor and saturation current of the diode as well as a light-induced R_p contribution. The latter could come from photoconductivity of the donor and/or acceptor layers.[7]

The measured J_{ph} versus V characteristics for the two different interfacial devices under investigation are presented in Fig. 3(b). In the inset of Fig. 3(b), J_{ph} is plotted against the effective voltage across the device, V_C–V, where V_C is the compensation voltage defined as the voltage where $J_{ph} = 0$. V_C is 0.62 V for device fabricated with a PEDOT:PSS interfacial layer, while $V_C = 0.86$ V for a MoO_3 interfacial layer device. We note that a scaling factor of 0.75 was used to multiply J_{ph} for the MoO_3 devices. Surprisingly, the shape of the photocurrent for both devices is nearly identical demonstrating that the photocurrent generated within the device is determined by the effective voltage, V_C–V, consistent with the absence of space-charge formation in the donor and acceptor layers. Thus, the differences that we observe in the J_{ph}–V curves can be attributed to the differences in the built-in field imposed by the presence of the anode interfacial layers. To gain further insight into the origin of the V_{OC}, we explore the photovoltaic characteristics of both devices at various temperatures and intensities of the incident light.

3.2 *Temperature and Power Dependence of the Open-Circuit Voltage*

Figure 4 compares the temperature dependence of the open-circuit voltage for both devices under different illumination intensities. For a given incident illumination intensity, we observe a linear increase in V_{OC} as the temperature decreases from 300 to 140 K. A maximum value for V_{OC} is achieved at ~140 K in both devices. Figure 4 shows this value is 1.05 V for the device fabricated with MoO_3 layer [Fig. 4(a)], whereas it is 0.65 V for the device with the PEDOT:PSS interfacial layer [Fig. 4(b)]. These observations indicate that the maximum V_{OC} value is strongly dependent on the nature of the anodic interfacial layer, while its position on the temperature scale seems to be determined by the properties of the donor/acceptor heterojunction. Upon further cooling, we observe a decrease in V_{OC} for both devices. The insets show the comparison of the temperature dependence of V_{OC} and the compensation voltage, V_C, in both devices. V_{OC} coincides with V_C for $T < 140$ K with both decreasing by nearly the same value of ~0.1 V at the lowest temperature. For $T > 140$ K, $V_{OC} < V_C$ with the MoO_3 device manifesting a larger offset than that of the PEDOT:PSS device.

Figure 4 also reveals a clear dependence of V_{OC} on the incident light intensity that is observed for $T > 140$ K in both devices. At <140 K, this power dependence disappears. Figure 5(a) presents a semilogarithmic plot of V_{OC} versus P, where P is the incident light intensity at three representative temperatures. The experimental data can be fitted with a linear function, and the slope can be compared to k_BT/q. The extracted slope decreases rapidly with temperature from $1.20k_BT/q$ ($0.80k_BT/q$) at $T = 290$ K to $0.92\ k_BT/q$ ($0.69k_BT/q$) when $T = 200$ K and $0.52k_BT/q$ ($0.47k_BT/q$) at $T = 150$ K for the MoO_3 (PEDOT:PSS) device. Equation (2) relates the observed power dependence of V_{OC} to that of $J_{ph}(V_{OC})$. Assuming that the measured photocurrent at $V = V_{OC}$ obeys the power-law dependence, $J_{ph}(V_{OC}) = J_T(P/P_o)^\alpha$, where the parameter J_T

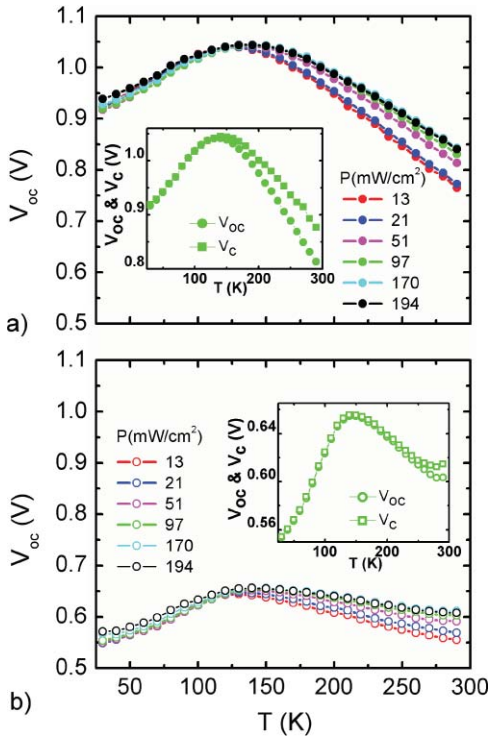

Fig. 4 Open-circuit voltage as a function of temperature for AlPcCl/C_{60} devices with (a) MoO_3 and (b) PEDOT:PSS interfacial layers under AM 1.5 Global solar simulator with various incident power intensity. The inset compares the temperature dependence of the open-circuit voltage (V_{OC}) and the compensation voltage (V_C) for $P = 97$ mW/cm^2.

depends only on temperature, then V_{OC} is given by

$$V_{OC} \simeq \frac{nk_BT}{q} \ln\left(\frac{J_T\left(P/P_O\right)^{\alpha}}{J_S}\right) = \frac{nk_BT}{q}\left(\alpha \ln\frac{P}{P_O} + \ln\frac{J_T}{J_S}\right). \quad (4)$$

Figure 5(b) shows a double-logarithmic plot of $J_{ph}(V_{OC})$ versus P. We observe an experimental power low dependence of $J_{ph}(V_{OC})$ with the exponent strongly decreasing with temperature. Extracting α from Fig. 5(b) and combined with the slope of V_{OC} versus ln(P) determined from Fig. 5(a), the diode ideality factor can be obtained using Eq. (4). The results of this analysis at various temperatures and their comparison to n derived from the J_d versus V characteristics are displayed in Fig. 6. Good agreement between the two values of n is illustrated in Fig. 6, corroborating our assumption of the power-law dependence of $J_{ph}(V_{OC})$ with P as well as demonstrating that the equivalent circuit model is a good representation of the data.

3.3 *Discussion*

We have shown above that the observed variation in V_{OC} associated with different interfacial layers at the anode of AlClPc/C_{60} bilayer organic photovoltaic devices is related to the diode saturation current density J_s. Earlier works on inorganic *p-n* homojunctions and heterojunctions have shown that J_s results from the dominant transport process associated with the *p-n* junction.[8] For devices with finite thickness, recombination at the electrode interfaces can also influence J_s. In *p-n* homojunctions, finite thickness correction leads to $J_s = J_{SO}F$, where J_{SO} is the saturation

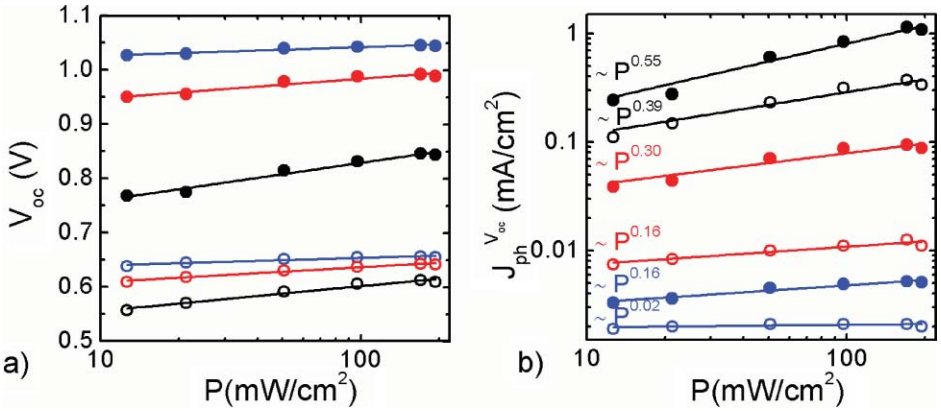

Fig. 5 Incident power (P) dependence of the open-circuit voltage (V_{OC}) (a) and the photocurrent at $V = V_{OC}$ [$J_{ph}(V_{OC})$] at three representative temperatures: $T = 290$ K (black), 200 K (red), and 150 K (blue). The solid circles are for the MoO_3 device, and the open-circles are for the PEDOT:PSS device.

current density for an infinitely thick diode and

$$F = \frac{S\cosh(W/L) + (D/L)\sinh(W/L)}{(D/L)\cosh(W/L) + S\sinh(W/L)}, \tag{5}$$

where W is the depletion width associated with the band-bending at the p-n junction, S is the surface recombination velocity at the electrode interface, and D and L are the diffusion coefficient and diffusion length of the minority carrier at the interface.[9] Applying Eq. (5) for the organic heterojunction with $W \ll L$ (Ref. 10), then $J_s \approx (J_{SO}L/D)S$. Recall that J_s is nearly two orders of magnitude lower in the device with the MoO_3 interface than that with the PEDOT:PSS interface. In the approximate expression for J_s, the quantities J_{SO}, L, and D are the same in both devices. Thus, S at the MoO_3/AlClPc interface is significantly lower than the one associated with the PEDOT:PSS/AlClPc interface. Such difference between the surface recombination velocities of the respective interfaces accounts for the variation in the open-circuit voltage observed in AlClPc/C_{60} bilayer photovoltaic devices.

An early work by Rand *et al.*[7] demonstrated that, in bilayer organic photovoltaic devices, V_{OC} approaches its maximum value at low temperatures. Our current work demonstrates that this maximum value coincides with the compensation voltage V_C. Malliaras *et al.*[11] showed that V_C at low temperatures is a measure of the diode built-in potential V_{bi}. We find that V_{bi} is higher

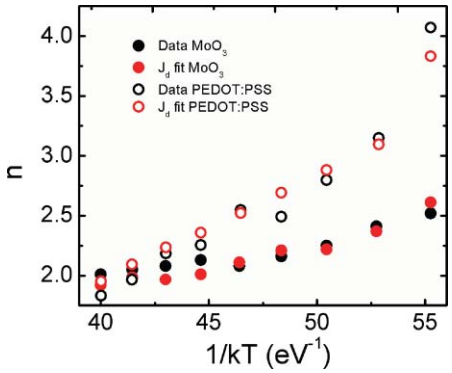

Fig. 6 Comparison of the diode ideality factor obtained from the data in Fig. 5 using Eq. (4) and from the fit of the J_d versus V using Eq. (1).

in the device where MoO_3 is used as an interfacial layer. Neglecting excitonic corrections, the maximum V_{OC} (or V_{bi}) in organic photovoltaic devices is given by the difference between the energetic positions of the donor highest-occupied molecular orbital (E_{HOMO}) and the acceptor lowest-unoccupied molecular orbital (E_{LUMO}) (Refs. 7 and 12). Measurements using ultraviolet photoelectron spectroscopy report values of 5.3 eV (Ref. 2) and 5.4 eV Ref. 1) for E_{HOMO} in AlPcCl and 4.1 eV Ref. 13) and 4.5 eV (Refs. 1 and 2) for E_{LUMO} in C_{60}. These values suggest that the maximum attainable V_{OC} for AlPcCl/C_{60} heterojunction devices is $\sim$ 0.8 to 1.3 V. The data in Fig. 4 illustrate that this expected maximum V_{OC} is achieved in the MoO_3 device in which it is observed that $V_{OC} = 1.05$ V at $T = 140$ K, indicating negligible voltage losses at the MoO_3/AlPcCl interface. The observed higher maximum V_{OC} (and V_{bi}) in the MoO_3 device compared to that in the PEDOT:PSS device is consistent with the low surface recombination velocity in the former as described earlier.

An unusual feature of the data presented in Fig. 4 is the apparent peak seen in the V_{OC} versus T curves at $T = 140$ K in both devices. Both devices manifest a drop from this peak V_{OC} value by about $\delta V_{OC} = 0.1$ V as the temperature is lowered to $T = 30$ K, suggesting that the effect is associated with the *p-n* heterojunction at the AlPcCl/C_{60} interface. This observation indicates a voltage loss contribution of the AlPcCl/C_{60} heterojunction to V_{OC}. We argue that the presence of photoexcited charge carriers at high temperatures screens the electrostatic band bending at this *p-n* heterojunction reducing its deleterious effect on V_{OC}.

4 Conclusions

The variation in the open-circuit voltage associated with different anode interface layers in chloroaluminum phthalocyanine/fullerene bilayer organic photovoltaic devices is shown to arise from interface charge recombination rather than from the intrinsic properties of the AlPcCl/C_{60} donor/acceptor heterojunction. Low surface recombination velocity is achieved at the interface formed by aluminum phthalocyanine chloride with molybdenum oxide accounting for the high V_{OC} in devices where MoO_3 is used as an interfacial layer.

References

1. R. F. Bailey-Salzman, B. P. Rand, and S. R. Forrest, "Near-infrared sensitive small molecule organic photovoltaic cells based on chloroaluminum phthalocyanine," *Appl. Phys. Lett.* **91**, 013508 (2007).
2. D. Y. Kim, F. So, and Y. Gao, "Aluminum phthalocyanine chloride/C_{60} organic photovoltaic cells with high open-circuit voltages," *Sol. Energy Mater. Sol. Cells* **93**, 1688–1691 (2009).
3. J. Subbiah, D. Y. Kim, and F. So, "The effect of molybdenum oxide interlayer on organic photovoltaic cells," *Proc. SPIE* **7416**, 74161W (2009).
4. W. Shockley and H. J. Queisser, "Detailed balance limit of efficiency of $_{p\text{-}n}$ Junction solar cells," *J. Appl. Phys.* **32**, 510–519 (1961).
5. M. A. Green, "Solar cell fill factors: general graph and empirical expressions," *Solid State Electron.* **24**, 788–789 (1981).
6. S. Yoo, B. Domercq, and B. Kippelen, "Intensity-dependent equivalent circuit parameters of organic solar cells based on pentacene and C_{60}," *J. Appl. Phys.* **97**, 103706 (2005).
7. B. P. Rand, D. P. Burk, and S. R. Forrest, "Offset energies at organic semiconductor heterojunctions and their influence on the open-circuit voltage of thin-film solar cells," *Phys. Rev. B* **75**, 115327 (2007).
8. S. M. Sze, *Physics of Semiconductor Devices*, Wiley, Hoboken, NJ (1981).
9. M. A. Green, *Solar Cells: Operating Priciples, Technology, and System Applications*, Prentice-Hall, Englewood Cliffs, NJ (1982).
10. F. Nuesch, M. Carrara, M. Schaer, D. B. Romero, and L. Zuppiroli, "The role of copper phthalocyanine for charge injection into organic light emitting devices," *Chem. Phys. Lett.* **347**, 311–317 (2001).

11. G. G. Malliaras, J. R. Salem, P. J. Brock, and J. C. Scott, "Photovoltaic measurement of the built-in potential in organic light emitting diodes and photodiodes," *J. Appl. Phys.* **84**, 1583–1587 (1998).
12. M. F. Lo, T. W. Ng, T. Z. Liu, A. L. Roy, S. L. Lai, M. K. Fung, C. S. Lee, and S. T. Lee, "Limits of open circuit voltage in organic photovoltaic devices," *Appl. Phys. Lett.* **96** 113303 (2010).
13. J. X. Tang, Y. C. Zhou, Z. T. Liu, C. S. Lee, and S. T. Lee, "Interfacial electronic structures in an organic double-heterostructure photovoltaic cell," *Appl. Phys. Lett.* **93**, 043512 (2008).